Chapter 15
Sulphur Compounds

Tjarda J. Roberts

This chapter presents a review of electrochemical sensors applied to the detection of sulphur compounds in the atmosphere, with a focus on environmental analysis of volcanic emissions of H_2S and SO_2. It describes the application to environmental monitoring of low-cost, low-power, miniature electrochemical sensors, originally developed for use in gas leak alarm systems within industry and for occupational health and safety monitoring systems. Over the last decade, such miniature electrochemical sensors have begun to be applied to real-time environmental monitoring of pollutants, including the characterisation of volcanic sulphurous emissions. This review outlines the principles of electrochemical sensor detection of volcanic gases, and highlights recent advances made in volcano hazard monitoring by using electrochemical sensors within multi-gas in situ measurement systems. A critical view on sources of measurement error in the characterisation of pollution plumes by electrochemical (and other) in situ sensors is presented, including the challenges imposed by sensor cross-sensitivities and finite sensor response within complex plume environments. Finally, future directions in this field are outlined, including the application of miniature electrochemical sensors to the monitoring of urban pollution, and sensor deployment on novel platforms such as balloon or unmanned aerial vehicle.

T.J. Roberts (✉)
LPC2E, UMR 7328, CNRS-Université d'Orléans, 3A avenue de la Recherche Scientifique, 45071 Orléans, Cedex 2, France
e-mail: Tjarda.Roberts@cnrs-orleans.fr; TjardaRoberts@gmail.com

L.M. Moretto, K. Kalcher (eds.), *Environmental Analysis by Electrochemical Sensors and Biosensors*, DOI 10.1007/978-1-4939-1301-5_15

15.1 Introduction

15.1.1 Sources of Sulphur to the Atmosphere

Sulphur is found in the atmosphere predominantly in the form SO_2, at typical abundances of pptv to ppbv. Elevated concentrations may occur near source emissions, or in cities where SO_2 contributes to photochemical smog pollution: a public health concern. SO_2 becomes oxidised to sulphuric acid (sulphate) aerosols in the atmosphere, with significant effects on regional and global climate, as well as ecosystems through sulphuric acid deposition. Atmospheric sulphur originates from both anthropogenic and natural sources, with anthropogenic emissions (60–100 Mt (S) $year^{-1}$) estimated to represent about 70 % of present-day global sulphur emissions [(1] and references therein). A major anthropogenic source is the burning of fossil fuels (as coal and crude oil deposits commonly contain 1–2 % sulphur by weight), in power stations, and from ship and road transport.[2] Smelting of metal sulphur ores can also be a strong localised source of atmospheric sulphur. Natural sources contribute the remaining 30 % of global sulphur emissions. These include an oceanic source (13–36 Mt(S) $year^{-1}$), volcanoes (6–20 Mt(S) $year^{-1}$), biomass burning (1–6 Mt(S) $year^{-1}$) and land biota and soils (0.4–5.6 Mt(S) $year^{-1}$). The oceanic source consists of oceanic plankton that release dimethyl sulphide (CH_3SCH_3) to the marine boundary layer, and sea spray which is a source of sulphate aerosol. The volcanic source consists principally of SO_2 and H_2S (as well as smaller quantities of OCS and H_2SO_4), which become oxidised to SO_2 and sulphate aerosol in the atmosphere. Wildfires (arguably both a natural and anthropogenic phenomenon) are also a source of SO_2, whilst decomposition of biological matter in soils, especially through anaerobic decomposition, leads to the emission of H_2S, which becomes oxidised to SO_2 in the atmosphere.

The balance between anthropogenic and natural sources has changed over time. Anthropogenic emissions from Europe and North America have declined in recent years following legislative action and the introduction of new technologies such as flue gas desulphurisation (FGD). Mareckova et al.[3] estimate that over the period 1990–2010, annual SO_x emissions declined from 21 to 15 Tg for the USA, and from 25 to 5 Tg for the European Union. Declining trends are also evident in the occurrence of acid rain, and in records of sulphur (but not reactive nitrogen) pollution that undergoes long-range transport followed by deposition in the Arctic[4,5)]. Conversely, annual SO_2 emissions from China were relatively stable or declining during the 1990s but increased by 50 % over 2000–2006 to reach 33 Tg due to rapid economic growth and energy consumption.[6] Since 2006, legislative and industry pollution reduction measures such as FGS have successfully reduced SO_2 emissions in China.

15.1.2 Health Impacts and Exposure Limits to Sulphurous Gases

Both SO_2 and H_2S are highly toxic to health, and exposure to their oxidation product, sulphuric acid aerosol—particularly fine particles (PM2.5, having diameter of 2.5 μm or less)—is also associated with adverse health impacts. SO_2 and sulphate aerosol exposure causes increased airway resistance, with asthma sufferers being particularly susceptible. WHO (World Health Organisation) guidelines recommend short-term SO_2 exposure should not exceed 500 μg/m^3 over 10 min whilst the long-term average exposure limit has recently been revised downwards from 125 to 20 μg/m^3 over 24 h.[7] H_2S affects the nervous system, causing eye irritation at 15 mg/m^3 (9 ppmv) and serious eye damage at 70 mg/m^3 (43 ppmv), and concentrations above 400 mg/m^3 (250 ppmv) can cause unconsciousness and death. The WHO-recommended average exposure limit for H_2S is 0.15 mg/m^3 over 24 h, with a recommended 30-min 7 μg/m^3 maximum to avoid odour annoyance in the general population, noting its characteristic 'rotten egg' odour.

Exposure to sulphurous and other toxic gases at high concentrations is of particular concern within industry, where accidental gas release can present a significant occupational exposure hazard. For example, hydrogen sulphide is formed as a by-product whenever sulphur-containing compounds come into contact with organic materials at high temperatures, such as in wastewater treatment, in wood pulp production (using the sulphate method), during coke production, in the manufacture of viscose rayon and in the tanning industry.[8] H_2S exposure is also a significant hazard in the oil and gas industry; natural gas deposits can contain up to 40 % hydrogen sulphide, and in work related to the treatment of sewage and farm slurry. An accident at a natural gas-treatment plant in Poza Rica, Mexico, in 1950 resulted in a major hydrogen sulphide gas leak (likely several thousands of ppmv), with 22 killed and 320 hospitalized (WHO air quality guidelines for Europe[7] and references therein). Such very large gas releases are rare, but occasional H_2S exposure to industry workers is not uncommon. In the UK, there is potential H_2S exposure to an estimated 125,000 workers in the treatment of sewage, effluent waste and farm slurry, and 3,000 workers in the offshore oil and gas industries. Industry H_2S exposure limits of 5 ppm (8 h average) and 10 ppm (short-term 15-min exposure limit) are currently recommended in the UK.[8]

15.1.3 Electrochemical Detection of Toxic Gases Within Industry

To improve industry safety, a range of electrochemical sensors that detect toxic gases have been developed. Such sensors can be used for flue gas emission testing. They are integrated into industry sites as part of gas leak alarm systems, which trigger an alarm if gas is detected above a particular threshold, enabling rapid

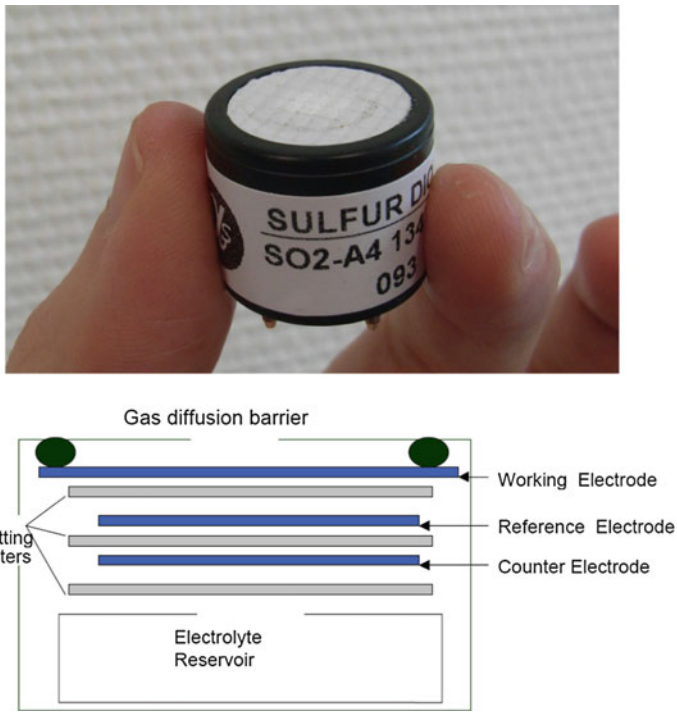

Fig. 15.1 Photograph of miniature (cm-sized) electrochemical sensor, and sensor diagram (image supplied by *Alphasense Ltd*)

evacuation following a gas leak, and a toxic hazard safety team to be directly dispatched to the polluted area. Output from such electrochemical sensors can also be monitored over time to assess variations in on-site gas exposure. A range of electrochemical sensors are commercially available to detect gases such as CO, H_2, HCl, NH_3 as well as H_2S and SO_2. Sensor company Interscan has developed portable (2 kg) electrochemical-sensor-based instruments with integrated sample-draw pump, capable of detecting ppmv and sub-ppmv concentrations of H_2S or SO_2. Sensor technology companies such as Alphasense Ltd, CityTech and Membrapor have developed miniature electrochemical sensors to detect toxic gases (including SO_2 and H_2S). The small size of these sensors—just a few cm and less than 10 g—enables such sensor alarm systems to be worn by the industry workers, thus providing industry exposure estimates on an individual level. Figure 15.1 illustrates the miniature size of these electrochemical sensors. The sensor's three electrodes are separated by wetting filters that allow capillary transport of the electrolyte (typically $H_2SO_{4(aq)}$). Gas diffusion into the cell leads to reactions at the working and counter electrodes. A general review is given by Stetter and Li,[9] highlighting the key working electrode reactions for SO_2 and H_2S electrochemical sensors: $SO_2 + 2H_2O \rightarrow {SO_4}^{2-} + 4H^+ + 2e^-$ and $H_2S + 4H_2O \rightarrow {SO_4}^{2-} + 10H^+ + 8e^-$, respectively. The electrochemical current thereby generated is proportional to the rate of gas

diffusion, hence gas mixing ratio abundance in the ambient atmosphere. For more details see manufacturers' websites (www.alphasense.com, www.citytech.com, www.membrapor.com).

15.1.4 Sulphur Gas Detection for Volcano Monitoring and Impact Assessment

During the last decade, the abovementioned portable electrochemical instrument and miniature electrochemical sensors have also been applied to environmental pollution monitoring within a research context. The low cost, low power and small size of the electrochemical sensors present advantages for the monitoring of gases in remote, challenging-to-access regions, where power supply is limited. In particular, the sensors have been applied to quantify sulphurous emissions from the remote summits of volcanoes. Volcanoes release a range of gases and aerosols, including H_2O, CO_2, SO_2, HCl, H_2S, SO_4^{2-}, OCS, HBr, HI, Hg and trace metals (in decreasing order of abundance). The major volcanic sulphurous emissions, SO_2 and H_2S, typically reach several to tens or hundreds of ppmv at the volcano crater rim, and thus are readily detectable by electrochemical sensor in the near-source or downwind plume.

The technological advance such electrochemical sensors bring to the monitoring, characterisation and quantification of volcano gas emissions is of interest to both volcanology and environmental science. Volcanologists monitor the composition and flux of volcano gas emissions in order to understand the subsurface process; a review for volcanic sulphur is provided by Oppenheimer et al.[10] Temporal changes in the observed volcanic sulphur emissions—both in terms of gas flux and gas composition—can provide predictive indications of changes in volcanic eruptive activity. Thus, monitoring of the volcanic gas emissions facilitates understanding of the subsurface magmatic conditions and can contribute to early-warning systems for volcanic unrest.

Observations of volcanic emissions are also integral to the assessment of plume atmospheric and ecological impacts, on local to global scales. Approximately 40 % of volcanic emissions are continuously released from persistently degassing volcanoes, into the lower-mid troposphere.[11] At low altitudes, such emissions impact local air quality (e.g. resulting in sulphurous volcanic smog, or VOG episodes of poor air quality[12)] and cause ecological damage (e.g. impacting a 22 km^2 zone downwind of Masaya volcano, Nicaragua, according to reference [(13)]. For volcanoes that have high altitude summits (e.g. Mt Etna, 3,300 m a.s.l.), the emission enters directly into the free troposphere, which limits the extent of a local impact but results in a prolonged atmospheric lifetime of the emission. Approximately 60 % of global volcanic emissions are released during explosive eruptions (such as Mt Pinatubo, 15 June 1991) that inject gases directly into the mid-upper troposphere or stratosphere. At stratospheric altitudes, inter-hemispheric dispersion and

oxidation of volcanic SO_2 to sunlight-scattering sulphate aerosol can lead to significant climate impacts.[14]

Thus, there is a strong interest in incorporating new low-cost, low-power electrochemical gas-sensing techniques to volcanic gas detection. Within volcano-monitoring networks, electrochemical sensors offer the potential for automated in situ monitoring of gas concentrations at the volcano summit, with wireless data transfer to the observatory in real time. This contrasts to traditional more labour-intensive methods for in situ gas sampling, involving sample collection by alkaline bottle or filter trap,[15] followed by laboratory analysis. Electrochemical sensors deployed on airborne platforms can also be used to detect the composition of the volcanic emission, and also map the plume dispersion[16,17] and study in-plume chemical processing,[18] thereby contributing observational data to support plume impact assessment.

15.2 Electrochemical Sensing of Volcanic Gas Emissions

15.2.1 Development of "Multi-Gas" in Situ Volcanic Gas Measurement Systems

The first application of a commercial (*Interscan*) H_2S instrument to volcanic gas detection was demonstrated by McGee et al.,[16] and was followed by further ground-based and airborne applications of this portable (2 kg) instrument to measure H_2S and SO_2 at a range of volcanoes.[17–21] In particular, these studies have demonstrated the capability of airborne plume mapping using electrochemical sensor instruments alongside other in situ sensors. Of growing interest is the application of miniature electrochemical sensors to detect volcanic gases, due to their small size (few cm and ~10 g), low cost and low power requirements. Such miniature electrochemical sensors have been integrated alongside other small sensors into backpack-sized portable sensing systems. The first so-called multi-gas system was developed by Shinohara[22] followed by numerous further volcanic applications.[23–42]

Table 15.1 summarizes notable developments in multi-gas instrumentation and volcanic electrochemical sensor deployments over the past decade. The first multi-gas system contained an electrochemical sensor for SO_2 and a CO_2 sensor based on infra-red spectroscopy.[22] Subsequent multi-gas instrument developments include the incorporation of an additional electrochemical sensor for H_2S,[28,37] and infra-red spectroscopic detection of H_2O alongside CO_2.[23,25,32] Recently, electrochemical sensor detection of volcanic H_2 has been demonstrated,[33] as well as CO and HCl.[42] The multi-gas systems have also been deployed alongside other in situ sensors, e.g. references [36, 37] and instrument miniaturisation has recently allowed deployment on novel platforms.[25,39,40,43]

Deployment of a multi-gas system to analyse gas emissions from the fumaroles of La Fossa crater, Vulcano, Italy, is illustrated in Fig. 15.2a. To make in situ

Table 15.1 Overview of multi-gas instruments that incorporate electrochemical sensors for in situ detection of volcanic gases as portable "backpack" and fixed-installation instruments, as well as commercial instruments based on electrochemical sensing techniques

Gases detected	Method	Comments	
SO_2	Commercial electrochemical instrument	Airborne, in the plume of Mt. Baker (USA)	16
SO_2	As above	Heliborne, alongside CO_2 instrument (prototype sensor deployed), plume of Miyakejima (Japan)	19
SO_2	As above	Ground based, alongside CO_2 instrument, plume of Kilauea (Hawaii, USA)	20
SO_2	As above	Airborne, alongside CO_2 and H_2S sensors, plume of White Island volcano, New Zealand	21
H_2S, SO_2	As above	All measurements integrated in single data acquisition system, in the eruption plume of Mt. Redoubt	17
H_2S, SO_2	As above	Simultaneous measurements of in-plume ozone depletion, in eruption plume of Mt. Redoubt	18
SO_2 CO_2 Humidity (H_2O)	Electrochemical Infra-red Capacitance	First portable multi-gas system, deployed at Tarumae, Tokachi and Meakan volcanoes (Japan)	22
As above + H_2O	Infra-red	In plume of Villarrica (Chile)	23
As above		In Mt. Etna (Italy) plume	25
As above + H_2	Semi-conductor	Plumes of Meakandake and Kuchinoerabujima (Japan)	44,45
As above		Portable, deployed on UAV in plume of Shinmoedake (Japan)	25
SO_2, H_2S	Electrochemical	Direct-to-vent detection of Nisyros fumaroles (Greece)	26
CO_2	Infra-red	Long-term installation with data telemetry and remote operation	27
SO_2, H_2S CO_2 Humidity (H_2O)	Electrochemical Infra-red Capacitance	Portable system, chemical mapping of fumarolic emissions from Vulcano and Mt. Etna (Italy)	28,29
As above		Simultaneous Hg instrument in fumaroles at Vulcano (Italy)	30
As above + H_2O	H_2O infra-red	In plume of Mt. Etna (Italy)	31
As above		Long-term automated system with data telemetry at Stromboli (Italy)	32,34,35
As above + H_2	Electrochemical	In plume of Mt. Etna	33

(continued)

Table 15.1 (continued)

Gases detected	Method	Comments	
SO_2, H_2S	Electrochemical	Portable and simultaneous with Hg instrument, in plume of Masaya and Telica volcanoes, Nicaragua	[36]
CO_2 Humidity (H_2O)	Infra-red Capacitance	In the Tatun fumarole field (Taiwan)	[37]
SO_2, H_2S, CO	Electrochemical	Portable, Solfatar crater (Italy)	[38]
SO_2 CO_2	Electrochemical Infra-red	Deployed on UAV in fumarole plume from Vulcano (Italy)	[39]
SO_2 Humidity (H_2O)	Electrochemical Capacitance	Deployed on CMET Balloon in Kilauea plume (Hawaii)	[40]
SO_2, H_2S, CO, H_2, HCl	Electrochemical	Portable, deployed in plumes of Villarrica (Chile)	[41]
As above		In plume of Mt. Aso (Japan)	[42]
SO_2	Electrochemical	Portable, deployed on UAV in plume of Turrialba Volcano (Costa Rica)	[43]

measurements in such a polluted environment requires a gas mask to be worn, as plume sulphur gas concentrations that can reach several hundreds of ppmv. In fact, H_2S and SO_2 concentrations are sufficiently high to react and form a yellow sulphur deposit around the fumarole vents as seen in Fig. 15.2a. Details of the instrument design are shown in Fig. 15.2b. This multi-gas system contains a suite of electrochemical sensors (capable of detecting H_2S, SO_2, CO, H_2 and HCl) with the air flow drawn over the sensors (contained in small housing) by a miniature pump. The electrochemical sensors generate a current output (nA) that is stored every second using a handheld computer. A filter on the inlet removes particles in order to prolong the sensor and pump lifetime. The system is approximately 'shoe-box' sized and is powered by a 12 V battery. See reference [42] for further information.

An example of data obtained using this instrument at the crater rim of Aso volcano (also detecting fumarolic emissions) is shown in Fig. 15.3. The sensor current outputs show co-varying variations with time (all sensor currents are positive except for HCl which also exhibits a larger baseline drift). These variations reflect the exposure of the instrument to fluctuating plume concentrations, due to the complex wind fields at the volcano summit. Gas mixing ratio time series derived from the sensor current outputs are shown in Fig. 15.3 and show similar co-varying variations with time that reflects the temporal plume exposure. Scatter plots of these gases relative to plume tracer SO_2 are shown in Fig. 15.4, with linear regression used to identify the characteristic molar gas ratio, finding $H_2/SO_2 = 0.2$,

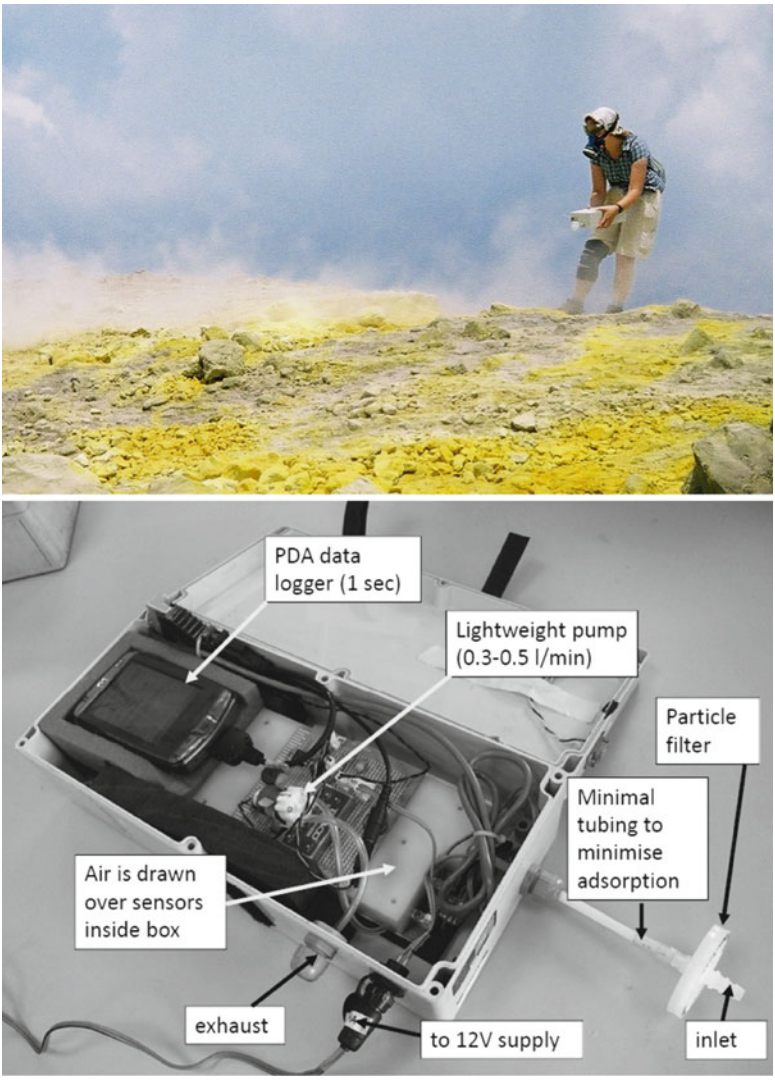

Fig. 15.2 *Upper*: Deployment of multi-gas instruments in fumaroles at Vulcano (Italy). *Lower*: Diagram of multi-gas instrument that includes six electrochemical sensors, as described by Roberts et al.[42]

$CO/SO_2 = 0.02$, for $H_2S/SO_2 = 0.15$, with estimated error of ± 0.01. These measurements show that under the reduced magmatic conditions of this fumarolic emission, reduced gases (such as H_2, H_2S and CO) are relatively abundant so as to be detectable. The general correlation with plume tracer SO_2 suggests limited in-plume chemistry of these species between their emission and detection (~minutes). Details of electrochemical sensor data analysis methodology are now discussed.

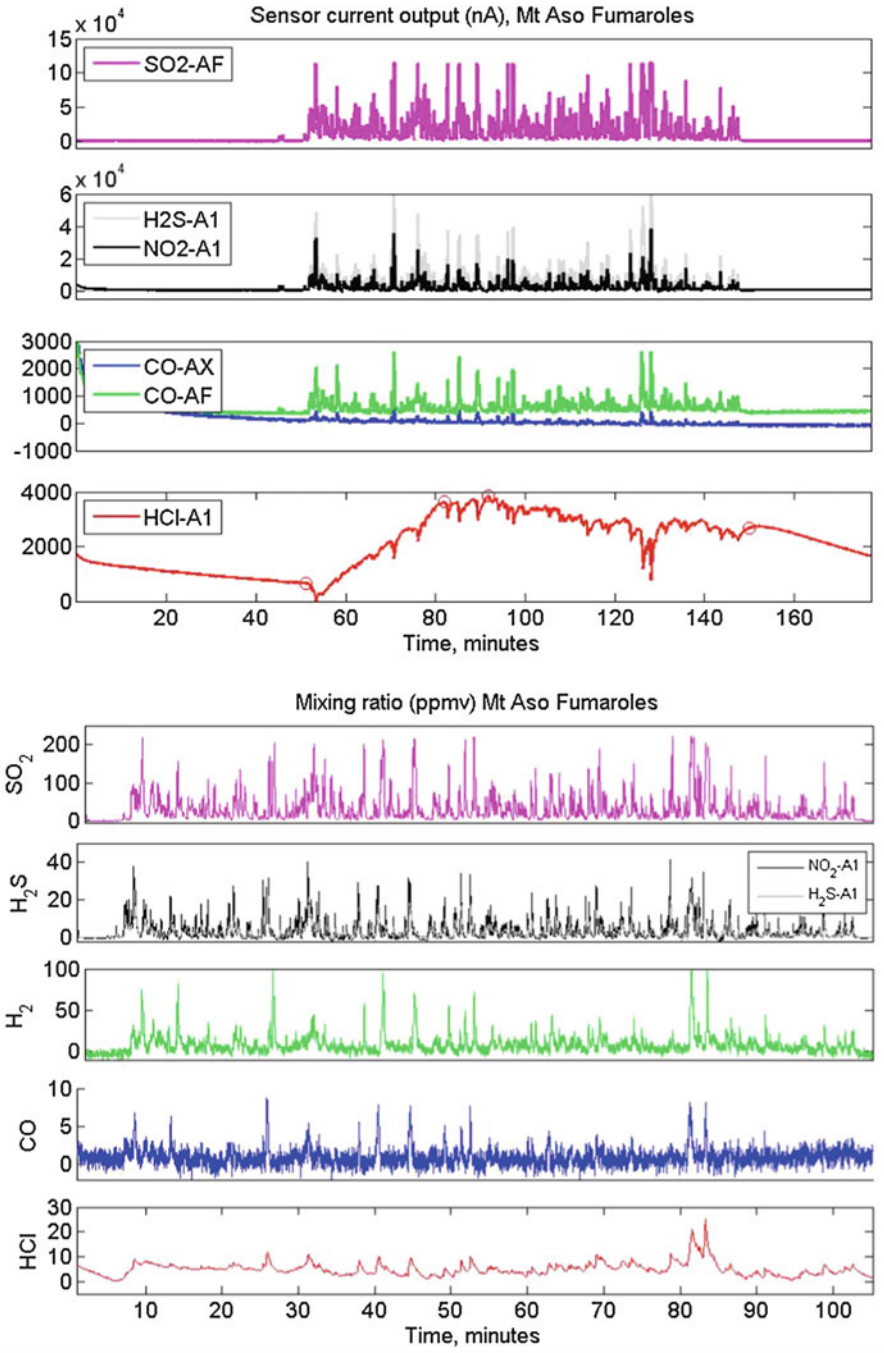

Fig. 15.3 *Upper figure*: Raw data showing 1 Hz time series of instrument output for electrochemical sensors SO2-AF, H2S-A1, NO2-A1, CO-AX, CO-AF and HCl-A1 at Aso volcano [42] for details). *Lower figure*: Processed data showing SO_2, H_2S, H_2, CO and HCl gas ppmv mixing ratio time series determined from analysis of the 1 Hz sensor signal

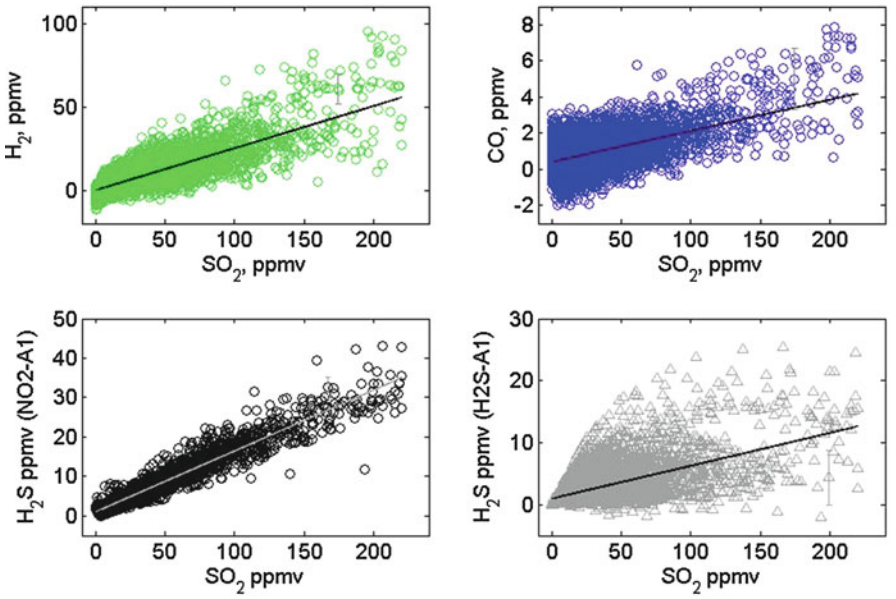

Fig. 15.4 Scatter plots of the gas mixing ratios derived from the electrochemical sensor data of Fig. 15.3, shown as X versus SO_2 where X is H_2, CO or H_2S. The estimate of H_2S from NO2-A1 sensor is preferred over that of H2S-A1 sensor which exhibits enhanced scatter: see text for explanation. Linear regression is used to determine the characteristic gas ratios in the Aso volcano fumarole emission

15.2.2 Data Analysis and the Importance of Sensor Cross-Sensitivities

Volcanic gas abundances encountered at the crater rim are sufficiently high (few to hundreds of ppmv) so as to be readily detected by electrochemical sensors, with the sensor current proportional to the gas abundance. However, the plume environment consists of a complex cocktail of volcanic gases that can cause interferences in the gas detection, and which must be removed during data post-processing. Electrochemical sensors for SO_2 typically do not exhibit significant cross-sensitivities to other volcanic gases (an integrated filter on the sensor prevents interferences from H_2S). Thus, Eq. (15.1) shows that the sensor output current, I_{SO2} (in nA), is related to the SO_2 mixing ratio, $[SO_2]$, by the sensor sensitivity, c_{SO2} (in nA/ppmv), a constant determined from laboratory calibration. The baseline current, B_{SO2}, may also need to be removed during data analysis, but can be readily determined during periods when the volcano plume is absent:

$$I_{SO2} = B_{SO2} + c_{SO2} \cdot [SO_2] \tag{15.1}$$

$$I_{H2S} = B_{H2S} + s_{H2S} \cdot [H_2S] + cs_{SO2} \cdot [SO_2] \tag{15.2}$$

However, electrochemical sensors for H_2S do tend to exhibit a cross-sensitivity to SO_2, of around 10–20 %. Thus the H_2S sensor current, Eq. (15.2), is a function of the baseline, B_{H2S}, the H_2S mixing ratio, $[H_2S]$, according to the sensor sensitivity, c_{H2S}, and also the SO_2 mixing ratio, $[SO_2]$, according to the sensor cross-sensitivity, cs_{SO2}. The interference from SO_2 can be removed during data post-processing, provided both the H_2S sensor sensitivity and cross-sensitivity are known, and by using the concurrent SO_2 mixing ratio determined from the SO_2 sensor. It is important that sensor cross-sensitivities are properly taken into account for accurate determination of plume gas ratios. For example, in a plume with $H_2S/SO_2 = 0.05$ gas ratio, failure to remove a 10 % cross-sensitivity of an H_2S sensor to SO_2 would lead to a measured gas ratio of 0.15, i.e. an error of 300 %. Alternatively, a filter may be applied to the specific sensor inlet to remove SO_2, e.g. references [44, 45]; however care must be taken that it does not co-remove H_2S.

Nevertheless, sensor cross-sensitivities can also bring new opportunities for gas measurement. Roberts et al.[42] deployed an NO_2 sensor in the plumes of Japanese volcanoes Aso and Miyakejima, and, noting that NO_2 concentrations were much less than H_2S, used the sensor's cross-sensitivity to measure H_2S abundance. The sensor presented advantages over traditional H_2S sensors because it did not exhibit a cross-sensitivity to SO_2, and also because the time-response of the NO_2 sensor (to H_2S) is more similar to the SO_2 sensor (see further discussion of measurement uncertainties below). In the same study[42] Roberts et al. also co-deployed two CO sensors, both of which exhibited cross-sensitivities to H_2. By co-analysing the two sensor outputs (which contrasted in their degree of cross-sensitivity), both CO and H_2 abundances could be determined in the volcanic plume.

15.2.3 Critical View on Sources of Multi-Gas Measurement Error

The accuracy of plume gas ratios reported from multi-gas systems depends on a number of factors influencing the sensor measurement error. These include sensor calibration, linearity and possible calibration drift, the sensor baseline and possible temperature, humidity and pressure dependences of the sensor output, as outlined below.

Of key importance is the sensitivity of the sensor current or voltage output, expressed as nA/ppmv or mV/ppmv of target gas, and any cross-sensitivity to nontarget gases, as mentioned above. These sensitivities are usually quantified by pre- and/or post-fieldwork laboratory calibrations where the sensor is exposed to a fixed concentration of gas. Such point calibrations assume linearity of the sensor responses to the target gases, which is generally a valid assumption; see, e.g., reference[42]. In order to reduce adverse effects from possible sensitivity drift, calibrations should be performed immediately prior to or after the fieldwork. Further, the laboratory calibrations performed at room temperature (~20–25 °C) and ambient pressure (~1 atm) do not necessarily reflect sensor properties at the

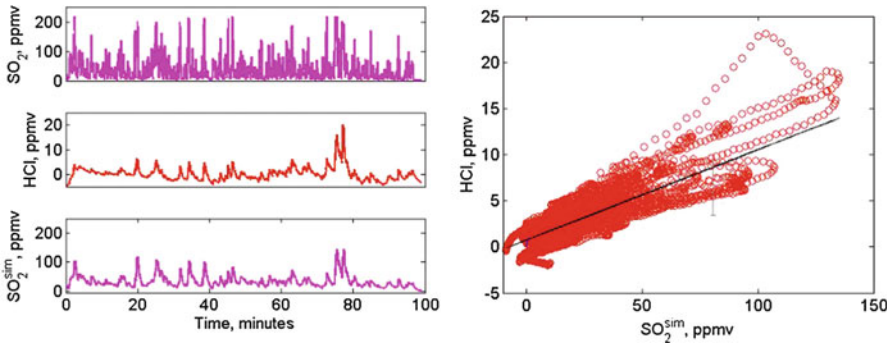

Fig. 15.5 The importance of sensor response time illustrated for HCl and SO_2 sensor pair. *Left*: SO_2 and HCl ppmv time series illustrated alongside a simulated *slow* SO_2 time series using E3, SO_2^{sim}. The latter has an improved correlation to HCl compared to the standard SO_2 time series. *Right*: Scatter plot of HCl versus simulated *slow* SO_2 time series used to derive an estimate for HCl/SO_2 ratio

temperature and pressure of the field measurements at the volcano summit (typically between a few hundred metres and 4 km altitude a.s.l.). Both atmospheric pressure and temperature decrease with altitude in the troposphere, the latter also varying diurnally and with season and latitude. Few studies have considered these effects on multi-gas measurements.

In addition to the above, it has recently been shown that the finite response time of the sensors is also a source of multi-gas measurement error, particularly in plumes with fluctuating gas abundance.[46] Direct comparison of output from sensors with contrasting response times can result in enhanced scatter and also bias in the derived volcanic gas ratios, and hence lead to inaccurate estimations of plume composition. Such errors are enhanced when interferences are removed in post-processing (e.g. for H_2S from the H_2S-A1 sensor in Fig. 15.2). Both data integration techniques[46] and sensor response modelling approaches[42] have been proposed to combat these measurement uncertainties. Sensors with vastly contrasting response times exhibit non-identical responses to fluctuating plume gas concentrations and thus cannot be compared directly. An example is the determination of HCl/SO_2 ratios from a fast SO_2 (~12 s response time) and slow HCl (approximately few minutes response time) sensor; Fig. 15.3[42] proposes the following sensor response modelling approach to analyse the data. A slower response SO_2 signal, SO_2^{SIM}, is first simulated from the fast response SO_2 output, SO_2^{FAST}, using Eq. (15.3) that is iteratively applied (beyond the starting value of $SO_2^{SIM}{}_{(t=1)}$ that is set to $SO_2^{FAST}{}_{(t=1)}$). The slowness factor, F, takes a value between 0 and 1, and can either be determined from laboratory measurements of sensor response time or inferred by optimising the correlation between the HCl sensor and SO_2^{SIM}. Figure 15.5 shows how the slow response SO_2 signal, SO_2^{SIM}, exhibits much greater similarity to the HCl sensor signal than the fast SO_2 measurement. Once the slow response SO_2 signal, SO_2^{SIM}, has been generated, it can be directly compared to the HCl sensor output, and a

scatter plot of HCl versus SO_2^{SIM} used to estimate the HCl/SO_2 ratio. For the fumaroles of Aso volcano, it was estimated that $HCl/SO_2 = 0.1 \pm 0.02$:

$$SO_2^{SIM}{}_{(t)} = F \cdot SO_2^{SIM}{}_{(t-1)} + (1 - F) \cdot SO_2^{FAST}{}_{(t)} \quad (15.3)$$

Further sensor response modelling approaches are in development for other multi-gas sensor pairs. In summary, it is emphasized that accurate determination of plume gas ratios from co-deployed in situ electrochemical (and other) sensors requires a consideration of sensor response times. Non-identical sensor response times can result in scatter and bias in the derived gas ratios, particularly in cases where cross-sensitivities need to be removed. Reported plume gas ratios from multi-gas instruments may need to be revisited in this context, and the effect is likely also important in the monitoring of other environments, such as urban pollution.

15.2.4 Insights Gained from Electrochemical Sensing of Volcanic Emissions

The growing application of electrochemical sensors to volcanic gas monitoring is bringing a wealth of new data on gas composition. Notwithstanding the abovementioned issues concerning measurement uncertainties, it is clear that electrochemical sensors bring new and valuable insights into volcanology, as highlighted by the examples below.

The volcanic plume composition, as quantified by the observed volcanic gas ratios, reflects the subsurface volcanic conditions. Partitioning between reduced and oxidised gases leads to characteristic H_2S/SO_2, CO/CO_2 and H_2/H_2O in the volcanic emission.[47] These gas ratios are dependent on the magmatic redox state, temperature and pressure, and thus can be used to infer subsurface magmatic plumbing scenarios. For example, Edmonds et al.[48] deployed a multi-gas electrochemical sensor system (including an electrochemical sensor for SO_2 alongside a separate in situ CO_2 (infrared sensor)) during the 2008–2010 summit eruption of Kilauea volcano, Hawaii. Analysis of the CO_2/SO_2 ratio was used to infer sub-surface magmatic plumbing during the eruption. The CO_2/SO_2 ratio in the main summit crater plume was lower than expected based on the previous eruptive history, yet during periods when the plume was absent (e.g. due to wind direction that advected it away from the sensors) CO_2-enriched (but SO_2 poor) air masses were occasionally observed. It was inferred that CO_2 accumulation at the magma chamber roof followed by diffuse degassing through permeable rock was likely responsible for this separation of volcanic sulphur and carbon emissions to the atmosphere.

Moreover, repeated or continuous monitoring of the volcanic emission chemical composition over time can provide useful insights into temporal changes in the subsurface magmatic processes. For example, Aiuppa et al.[34,35] used three fully automated multi-gas instruments at the summit of Mt. Stromboli, to measure CO_2 and SO_2 gas concentrations over several years. The observations were analysed to

yield CO_2/SO_2 time series as well as CO_2 fluxes. It was shown that major explosions at Stromboli are systematically preceded by a phase of increasing CO_2 degassing, with CO_2/SO_2 increasing from ~5 to >20. This finding is in agreement to conceptual models of volcanic degassing at Stromboli, indicating a subsurface separation and accumulation of CO_2-rich gas bubbles, whose episodical release results in an explosive event. This demonstrated capability of automated multi-gas monitoring systems to detect temporal changes in the plume gas ratio opens new promising perspectives for in situ electrochemical sensor methods in the forecasting of explosive volcanic events in future.

15.3 Future Directions for Miniature Electrochemical Sensors

15.3.1 Electrochemical Sensor Deployments on Novel Platforms

The lightweight, low-cost and low-power properties of miniature electrochemical sensors make the sensors very suitable for deployment on novel platforms such as unmanned aerial vehicle (UAV). Such platforms can be advantageous if deployment of in situ sensors is impractical due to a high risk of an imminent explosive volcanic eruption, or where the region of volcanic degassing cannot practically be accessed using a handheld instrument. Some recent volcanological applications are outlined below.

McGonigle et al.[39] presented the first study to use an in situ electrochemical sensor deployed on an unmanned aerial vehicle alongside an infra-red spectrometer to characterise CO_2 and SO_2 in the plume $\leq$200 m downwind of La Fossa, Vulcano, Italy. This study demonstrated the advantages of UAV-based sensing not only from a safety perspective (obtaining plume measurements with minimal personal gas exposure), but also to quantify the bulk plume emission arising from individual fumarole sources.

Shinohara[25] performed a UAV-based characterisation of the plume from Shinmoedake, Kirishima volcano, Japan, using electrochemical and other in situ sensors. Due to ongoing explosive eruptive activity, access to the volcano summit area 4 km around the volcano was restricted (even for manned aircraft). Therefore this study demonstrates UAVs as a viable method to obtain plume gas measurements under hazardous summit conditions. Several molar gas ratios were determined during a period with Vulcanian eruptions in May 2011, including $CO_2/SO_2 = 8$, $H_2O/CO_2 = 70$ and $H_2/SO_2 = 0.03$. It was found that plume SO_2/H_2S showed a decrease over March to May 2011 from 8 to 0.8, which is interpreted as resulting from an increase in degassing pressure of the volcano.

Pieri et al.[43] present measurements of SO_2 in the plume of Turrialba Volcano in Costa Rica for UAV flights that reach up to 3.5 km. This study demonstrates the first

routine (monthly deployments since 2013) UAV-based SO_2 data acquisition and are being used for validation of satellite SO_2 retrievals during ASTER (Advanced Spaceborne Thermal Emission and Reflection Radiometer, ASTER) overpasses. Pieri et al.[43] also provide an overview of reported UAV approaches to volcanic plume detection as well as tethered and meteorological balloon applications.

UAVs can also be used to explore the temporal evolution of the volcano plume chemistry. A novel CMET (controlled meteorological) balloon system[49] has been used to follow the trajectory of the Kilauea (Hawaii) plume to perform quasi-Lagrangian studies of the plume evolution. Observations from the payload that included an electrochemical SO_2 sensor as well temperature, pressure and humidity sensors[40] demonstrated correlation between SO_2 and humidity in the near-source plume, but appear to show anti-correlation further downwind, potentially due to in-plume processing.

Finally, the potential of in situ sensors upon airborne platforms to perform detailed plume characterisation and chemical mapping and to trace the chemical evolution of the plume with time is shown by Kelly et al.[18] who deployed an electrochemical SO_2 sensor alongside an ozone sensor based on UV spectroscopy on an instrumented aircraft. Through repeated transects across the plume, the dispersion of SO_2 downwind of the volcano could be mapped. Moreover, the ozone sensor identified rapid ozone depletion within the plume. This ozone depletion was attributed to rapid in-plume reactive halogen chemistry: numerical simulations using the *PlumeChem* model[50] were able to spatially reproduce the observed ozone depletion for the reported SO_2 flux and dispersion rate. It is anticipated that further advances in instrumented balloon and UAV technologies will allow airborne chemical mapping studies to become more frequent in future in order to probe the plume impact on downwind atmospheric chemistry, as well as quantify the emissions near source.

15.3.2 Improved Accuracy and Detection Limit: Applications Beyond Volcanoes

Improvements to the sensitivity and stability specifications of commercially available miniature electrochemical sensors have also brought the possibility to measure gases at ever lower concentrations, and the capability to detect pollutants in new environments. To improve resolution and detection limits, the miniature electrochemical sensors should be deployed using low noise electronics. Figure 15.6 (upper) illustrates the detection of SO_2 in the relatively dilute grounding plume from Mt. Etna, using high- and low-sensitivity electrochemical sensors logging at 1 Hz and 0.1 Hz, respectively, and low-noise electronics. The two sensors show very similar response to the plume gases, and are capable of observing sub-ppmv (tens to hundreds of ppbv) variations in SO_2 gas abundance. Baseline noise is lowest for the high-sensitivity sensor.

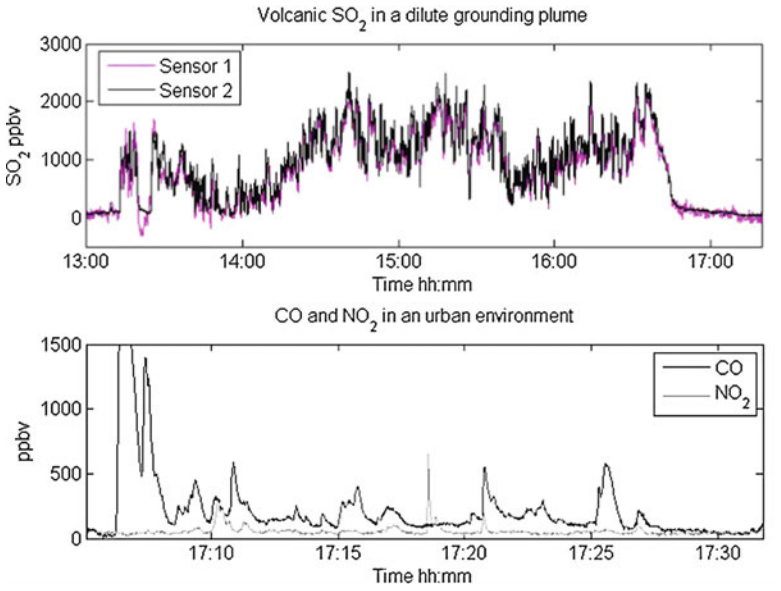

Fig. 15.6 *Upper*: SO_2 mixing ratio time series obtained in a dilute downwind volcanic plume using low-noise electronics, logging output from two non-identical miniature electrochemical SO_2 sensors with high sensitivity (black) and lower sensitivity (purple), at 1 Hz and 0.1 Hz, respectively. *Lower*: Mixing ratio abundances of excess (plume peaks - background) CO and NO_2 at a cross-roads in an urban environment (Orleans, France), measured at 1 Hz using low-noise electronics, with the high-sensitivity SO_2 sensor used to detect NO_2 (cross-sensitivity −120 %) alongside a high-sensitivity sensor for CO

Similar miniature electrochemical sensors have recently been applied to quantifying ozone, CO, NO and NO_2 pollution in an urban environment[51–53] in stationary networks as well as on moving (tramway, pedestrian, bicyclist) platforms. This potential for urban monitoring is demonstrated here through a short instrument deployment at urban cross-roads in Orleans (France). Figure 15.6 (lower) shows the electrochemical sensor response to emissions from passing traffic, where 'excess' CO and NO_2 are calculated by subtracting the constant background abundance. The SO_2 (high sensitivity) sensor is used here to detect NO_2 by means of its ~−120 % cross-sensitivity to this gas, whilst a CO sensor is used to detect CO. Note that in urban environments the SO_2 electrochemical sensor signal due to NO_2 greatly exceeds that due to volcanic sulphurous gases, in contrast to volcanic plumes. The measurements of Fig. 15.6 show fluctuations in excess NO_2 and CO abundance that exhibit a degree of independence, with the CO traffic signal generally exceeding NO_2. These observations are similar to the study of Mead et al.[53]

At low concentrations (e.g. towards background levels), the zero-gas baseline exerts a more significant influence on the sensor output current, and needs careful correction.[53] Issues of sensor cross-sensitivity also need to be considered, for example, the interferences of H_2 on the detection of CO. Future urban sensor networks may co-deploy additional sensors in order to extract these interferences,

in analogous manner to the approach demonstrated by Roberts et al.[42] regarding CO and H_2 in volcanic plumes. Measurement errors caused by finite sensor response to fluctuating gas abundances, as highlighted above, are also likely of quantitative importance in electrochemical sensing of urban pollution. Whilst these measurement uncertainties require further careful consideration, miniature electrochemical sensor technology appears a promising low-cost method for urban pollutant and personal health (as well as volcano) monitoring in future.

References

1. Stevenson DS, Johnson CE, Collins WJ, Derwent RG (2003) The tropospheric sulphur cycle and the role of volcanic SO_2. In: Clive O, David M, Pyle-Jenni B (eds) Volcanic degassing. Geological Society of London, London, ISBN 186239136X, 9781862391369
2. Smith SJ, van Aardenne J, Klimont Z, Andres RJ, Volke A, Delgado AS (2011) Anthropogenic sulphur dioxide emissions 1850–2005. Atmos Chem Phys 11:1101–1116. doi:10.5194/acp-11:1101-2011
3. Mareckova K, Wankmueller R, Whiting R, Pinterits M (2012) Review of emission data reported under the LRTAP Convention and NEC Directive. EMEP Inventory Review. http://www.ceip.at/review-results/
4. Hole LR, Christensen JH, Ruoho-Airola T, Torseth K, Ginzburg V, Glowacki P (2009) Past and future trends in concentrations of sulphur and nitrogen compounds in the Arctic. Atmos Environ 43:928–939
5. Kühnel R, Roberts TJ, Bjorkman MP, Isaksson E, Aas W, Holmen K, Strom J (2011) 20-year climatology of NO_3^- and NH_4^+ wet deposition at Ny-Alesund. Svalbard, Adv Meteorol. doi:10.1155/2011/406508, Article ID 406508
6. Lu Z, Streets DG, Zhang Q, Wang S, Carmichael GR, Cheng YF, Wei C, Chin M, Diehl T (2000) Tan Q (2010) Sulphur dioxide emissions in China and sulphur trends in East Asia since. Atmos Chem Phys 10:6311–6331
7. Krzyzanowski M, Cohen A (2008) Update of WHO air quality guidelines. Air Qual Atmos Health 1:7–13. doi 10.1007/s11869-008-0008-9. See also: WHO air quality guidelines for Europe, 2nd ed. WHO Regional Publications, European Series, No. 91 (2000). ISBN 92 890 1358 3. Ch 6.6: Hydrogen sulphide. Ch 7.4: Sulphur dioxide. WHO air quality guidelines for particulate matter, ozone, nitrogen dioxide and sulphur dioxide, Global update 2005. Summary of risk assessment. http://whqlibdoc.who.int/hq/2006/WHO_SDE_PHE_OEH_06.02_eng.pdf
8. Costigan MG (2003) Hydrogen sulphide: UK occupational exposure limits. Occup Environ Med 60:308–312
9. Stetter JR, Li J (2008) Amperometric gas sensors: a review. Chem Rev 108:352–366
10. Oppenheimer C, Scaillet B, Martin RS (2011) Sulphur degassing from volcanoes: source conditions, surveillance, plume chemistry and impacts. Rev Miner Geochem 73:363–421. doi:10.2138/rmg.2011.73.13
11. Halmer MM, Schmincke HU, Graf HF (2002) The annual volcanic gas input into the atmosphere, in particular into the stratosphere: a global data set for the past 100 years. J Volcanol Geotherm Res 115(3–4):511–528
12. Michaud JP, Krupitsky D, Grove JS, Anderson BS (2005) Volcano related atmospheric toxicants in Hilo and Hawaii volcanoes national park: implications for human health. Neurotoxicology 26(4):555–563
13. Delmelle P, Stix J, Baxter PJ, Garcia-Alvarez J, Barquero J (2002) Atmospheric dispersion, environmental effects and potential health hazard associated with the low-altitude gas plume of Masaya volcano, Nicaragua. Bull Volcanol 64(6):423–434

14. Robock A (2000) Volcanic eruptions and climate. Rev Geophys 38(2):191–219
15. Giggenbach WF (1975) A simple method for the collection and analysis of volcanic gas samples. Bull Volcanol 39:15–27
16. McGee KA, Doukas MP, Gerlach TM (2001) Quiescent hydrogen sulphide and carbon dioxide degassing from Mount Baker, Washington. Geophys Res Lett 28(23):4479–4482
17. Werner C, Kellu PJ, Doukas M, Lopez T, Pfeffer M, McGimsey R, Neal C (2013) Degassing of CO_2, SO_2, and H_2S associated with the 2009 eruption of Redoubt Volcano, Alaska. J Volcanol Geotherm Res 259:270–284
18. Kelly PJ, Kern C, Roberts TJ, Lopez T, Werner C, Aiuppa A (2013) Rapid chemical evolution of tropospheric volcanic emissions from Redoubt Volcano, Alaska, based on observations of ozone and halogen-containing gases. J Volcanol Geotherm Res 259:317–333
19. Shinohara H, Kazahaya K, Saito G, Fukui K, Odai M (2003) Variation of CO_2/SO_2 ratio in volcanic plumes of Miyakejima: stable degassing deduced from heliborne measurements. Geophys Res Lett 30(5):1208. doi:10.1029/2002GL016105
20. Hager SA, Gerlach TM, Wallace PJ (2008) Summit CO2 emission rates by the CO_2/SO_2 ratio method at Kīlauea Volcano, Hawaii, during a period of sustained inflation. J Volcanol Geotherm Res 177(4):875–882
21. Werner C, Hurst T, Scott B, Sherburn S, Christenson BW, Britten K, Cole-Baker J, Mullan B (2008) Variability of passive gas emissions, seismicity, and deformation during crater lake growth at White Island Volcano, New Zealand, 2002–2006. J Geophys Res 113, B01204. doi:10.1029/2007JB005094
22. Shinohara H (2005) A new technique to estimate volcanic gas composition: plume measurements with a portable multi-sensor system. J Volcanol Geotherm Res 143(4):319–333
23. Shinohara H, Witter JB (2005) Volcanic gases emitted during mild strombolian activity of Villarrica volcano, Chile. Geophys Res Lett 32:L20308. doi:10.1029/2005GL024131
24. Shinohara H, Aiuppa A, Giudice G, Gurrieri G, Liuzzo M (2008) Variation of H_2O/CO_2 and CO_2/SO_2 ratios of volcanic gases discharged by continuous degassing of Mount Etna volcano, Italy. J Geophys Res 113, B09203
25. Shinohara H (2013) Composition of volcanic gases emitted during repeating Vulcanian eruption stage of Shinmoedake, Kirishima volcano, Japan. Earth Planets Space 65:667–675
26. Teschner M, Vougioukalakis GE, Faber E, Poggenburg J, Hatziyannis G (2005) Real time monitoring of gas-geochemical parameters in Nisyros fumaroles. Dev Volcanol 7:247–254
27. Teschner M, Faber E, Poggenburg J, Vougioukalakis GE, Hatziyannis G (2007) Continuous, direct gas-geochemical monitoring in hydrothermal vents: installation and long-term operation on Nisyros Island (Greece). Pure Appl Geophys 164(12):2549–2571
28. Aiuppa A, Federico C, Giudice G, Gurrieri S (2005). Chemical mapping of a fumarolic field: La Fossa Crater, Vulcano Island (Aeolian Islands, Italy). Geophys Res Lett 32: L13309. doi:10.1029/2005GL023207
29. Aiuppa A, Federico C, Guidice G, Gurrieri S, Liuzzo M, Shinohara H, Favara,R, Valenza M (2006) Rates of carbon dioxide plume degassing from Mt Etna volcano. J Geophys Res 111: B09207. doi:10.1029/2006JB004307
30. Aiuppa A, Bagnato BE, Witt MJ, Mather TA, Parello F, Pyle DM, Martin RS (2007) Real-time simultaneous detection of volcanic Hg and SO_2 at La Fossa Crater, volcano (Aeolian Islands, Sicily). Geophys Res Lett 34(21), L21307
31. Aiuppa A, Giudice G, Gurrieri S, Liuzzo M, Burton M, Caltabiano T, McGonigle AJS, Salerno G, Shinohara H, Valenza M (2008) Total volatile flux from Mount Etna. Geophys Res Lett 35, L24302
32. Aiuppa A, Federico C, Giudice G, Giuffrida G, Guida R, Gurrieri S, Liuzzo M, Moretti R, Papale P (2009) The 2007 eruption of Stromboli volcano: Insights from real-time measurement of the volcanic gas plume CO_2/SO_2 ratio. J Volcanol Geotherm Res 182:221–230. doi:10.1016/j.jvolgeores.2008.09.013

33. Aiuppa A, Shinohara H, Tamburello G, Giudice G, Liuzzo M, Moretti R (2011a). Hydrogen in the gas plume of an open vent volcano, Mount Etna, Italy. J Geophys Res 116: B10204. doi:10.1029/2011JB008461
34. Aiuppa A, Burton M, Allard P, Caltabiano T, Guidice G, Gurrieri S, Liuzzo M, Salerno G (2011) First observational evidence for CO_2 driven origin of Stromboli's major explosions. Solid Earth 2:135–142
35. Aiuppa A, Bertagnini A, Métrich A, Di Muro A, Liuzzo M, Tamburello G (2010) A model of degassing for Stromboli volcano. Earth Planet Sci Lett 295(1–2):195–204
36. Witt MLI, Mather TA, Pyle DM, Aiuppa A, Bagnato E, Tsanev VI (2008) Mercury and halogen emissions from Masaya and Telica volcanoes, Nicaragua. J Geophys Res Solid Earth 113, B06203
37. Witt M, Fischer TP, Pyle DM, Yang TF, Zellmer GF (2008) Fumarole compositions and mercury emissions from the Tatun Volcanic Field, Taiwan: results from multi-component gas analyser, portable mercury spectrometer and direct sampling techniques. J Volcanol Geotherm Res 178(4):636–643
38. De Vito S, Massera E, Quercia L, Di Francia G (2007) Analysis of volcanic gases by means of electronic nose. Sensor Actuat B Chem 127(1):36–41
39. McGonigle AJS, Aiuppa A, Giudice G, Tamburello G, Hodson AJ, Gurrieri S (2008) Unmanned aerial vehicle measurements of volcanic carbon dioxide fluxes. Geophys Res Lett 35, L06303
40. Durant A, Voss P, Watson M, Roberts TJ, Thomas H, Prate F, Sutton J, Mather T, Witt M, Patrick M (2010) Real-time in situ measurements of volcanic plume physico-chemical properties using controlled METeorological balloons. EGU General Assembly 2010. 2–7 May 2010, Vienna, Austria, p. 4937
41. Sawyer GM, Salerno GG, Le Blond JS, Martin RS, Spampinato L, Roberts TJ, Mather TA, Witt MLI, Tsanev VI, Oppenheimer C (2011) Gas and aerosol emissions from Villarrica volcano, Chile. J Volcanol Geotherm Res 203:62–75
42. Roberts TJ, Braban CF, Oppenheimer C, Martin RS, Freshwater RA, Dawson DH, Griffiths PT, Cox RA, Saffell JR, Jones RL (2012) Electrochemical sensing of volcanic gases. Chem Geol 332–333:74–91
43. Pieri DD, Diaz JA, Bland G, Fladeland M, Madrigal Y, Corrales E, Alan A, Realmuto V, Miles T, Abtahi A (2013) In situ observations and sampling of volcanic emissions with Nasa and Ucr unmanned aircraft including a case study at Turrialba volcano, Costa Rica. In: Pyle DM, Mather TA, Biggs J (eds). Remote-sensing of volcanoes and volcanic processes: integrating observation and modelling. Geological Society, London. Geological Society Special Publication 380
44. Shinohara H, Matsushima N, Kazahaya K, Ohwada M (2011) Magma-hydrothermal system interaction inferred from volcanic gas measurements obtained during 2003–2008 at Meakandake volcano, Hokkaido, Japan. Bull Volcanol 73(4):409–421
45. Shinohara H, Hirabayashi J, Nogami K, Iguchi M (2011) Evolution of volcanic gas composition during repeated culmination of volcanic activity at Kuchinoerabujima volcano, Japan. J Volcanol Geotherm Res 202(1–2):107–116
46. Roberts TJ, Saffell JR, Oppenheimer C, Lurton T (2014). Electrochemical sensors applied to pollution monitoring: measurement error and gas ratio bias—a volcano plume case study. J Volcanol Geotherm Res 281:85–96
47. Gerlach TM, Nordlie BE (1975) The C\O\H\S gaseous system, part II: temperature, atomic composition, and molecular equilibria in volcanic gases. Am J Sci 275:377–394
48. Edmonds M, Sides IR, Swanson D, Werner C, Martin RS, Mather TA, Herd RA, Jones RL, Mead MI, Sawyer G, Roberts TJ, Sutton AJ, Elias T (2013) Magma storage, transport and degassing during the 2008-10 summit eruption at Kilauea Volcano, Hawaii. Geochim Cosmochim Acta 123:284–301. doi:10.1016/j.gca.2013.05.038

49. Voss PB, Hole LR, Helbling EF, Roberts TJ (2013) Continuous in-situ soundings in the arctic boundary layer: a new atmospheric measurement technique using controlled meteorological balloons. J Intell Robot Syst 70(1–4):609–617. doi:10.1007/s10846-012-9758-6
50. Roberts TJ, Braban CF, Martin RS, Oppenheimer C, Adams JW, Cox RA, Jones RL, Griffiths PT (2009) Modelling reactive halogen formation and ozone depletion in volcanic plumes. Chem Geol 263(1–4):151–163. doi:10.1016/j.chemgeo.2008.11.012
51. Hasenfratz D, Saukh O, Thiele L (2012) On-the-fly calibration of low-cost gas sensors. Wireless sensor networks. Springer, Berlin. pp. 228–244
52. Li JJ, Faltings B, Saukh O, Hasenfratz D, Beutel J (2012) Sensing the air we breathe—the OpenSense Zurich dataset. In: Proc. 26th int'l conf. on the advancement of artificial intelligence (AAAI '12). pp. 323–325
53. Mead IM, Popoola OAM, Stewart GB, Landshoff P, Calleja M, Hayes M, Baldovi JJ, McLeod MW, Hodgson TF, Dicks J, Lewis A, Cohen J, Baron R, Saffell JR, Jones RL (2013) The use of electrochemical sensors for monitoring urban air quality in low-cost, high-density networks. Atmos Environ 70:186–203